

# DETECTING CEREBRAL MICROBLEEDS IN 7.0 T MR IMAGES USING THE RADIAL SYMMETRY TRANSFORM

Hugo J. Kuijf<sup>1</sup>, Jeroen de Bresser<sup>1,2</sup>, Geert Jan Biessels<sup>2</sup>, Max A. Viergever<sup>1</sup>, Koen L. Vincken<sup>1</sup>

<sup>1</sup> Image Sciences Institute, University Medical Center Utrecht, Utrecht, The Netherlands

<sup>2</sup> Department of Neurology, University Medical Center Utrecht, Utrecht, The Netherlands

## ABSTRACT

Cerebral microbleeds have recently received an increased interest, because they appear to be markers of increased risk of vascular events and dementia. Detection and scoring of microbleeds currently requires extensive manual evaluation and hence is very time-consuming. The rating time may be significantly decreased by automated detection of microbleeds using the radial symmetry transform. The goal is to automatically detect cerebral microbleeds in high-resolution MR brain scans, while reducing the number of false positives that need to be removed afterwards by a human rater. A proof of principle experiment was performed and evaluated with two participants of whom cerebral microbleeds were scored by human raters. As an indication of what the proposed method may accomplish, the experiment showed that human rating time reduced from 30 to 1.5 minutes per participant.

**Index Terms**— cerebral microbleeds, radial symmetry transform, 7.0T brain MRI

## 1. INTRODUCTION

In recent years, there has been an increasing interest in cerebral microbleeds. They are seen as a distinct entity from larger hemorrhage. Cerebral microbleeds are associated with hypertensive vasculopathy, white matter hyperintensities and lacunar infarcts, and they are a key MRI marker of cerebral amyloid angiopathy [1, 2, 3, 4]. Microbleeds consist of hemosiderin deposits [5] that are paramagnetic and cause a local field inhomogeneity surrounding the microbleed in the magnetic field of an MR. They are visualized as round, hypointense spots using a T2\*-weighted gradient-recalled echo (GRE) MR sequence. Cerebral microbleeds are usually defined as having a diameter ranging from 2 to 10 mm [6], because the used 1.5T or 3.0T scan resolution does not permit detection of smaller microbleeds.

To date, cerebral microbleeds are visually detected on MR scans (typically  $576 \times 576 \times 333$  voxels). It takes a single rater about 30 minutes to detect all cerebral microbleeds in a single high resolution (7.0T) MR scan, given the difficulty of distinguishing microbleeds from the large amount of visible vessels. Although (semi-)automated detection of cerebral microbleeds is likely to reduce rating time significantly, no successful reports have been published yet. In this study we have performed a proof of principle experiment to investigate the possibility of automatically detecting all candidate microbleed locations from an MR brain scan, by means of a method based on the radial symmetry transform. The goal is to develop a system that has a very high sensitivity, while minimizing the number of false positives. Subsequently, only the false positives will have to be removed by the rater(s), which will reduce the rating time significantly.

## 2. METHODS AND MATERIALS

### 2.1. Participants

For this study, two participants (age: 61 and 71 years) with microbleeds and no other brain pathology (like infarcts) were included from the second manifestations of arterial disease (SMART) study [7]. The objectives of the SMART study are to determine the prevalence of vascular risk factors and concomitant arterial disease and to study the incidence of future cardiovascular events and its predictors in these high-risk patients. The SMART study and the 7.0T imaging were approved by the Medical Ethics Committee. Written informed consent was given by the participants.

### 2.2. MRI

MRI scans and post-processing were performed as described previously by Conijn *et al.* [8], on a 7.0T whole-body system (Philips Healthcare, Cleveland, OH). A dual echo T2\*-weighted sequence was acquired, with echo times of 2.5 ms for the first echo and 15.0 ms for the second echo. The repetition time was 20 ms. A flyback gradient was applied between the first and second readout. Sensitivity encoding (SENSE) was applied in the RL direction. The images were reconstructed to  $0.35 \times 0.35 \times 0.3$  mm<sup>3</sup> voxels and the built-in phase correction, partial-echo filter, and homogeneity correction of the MR system were applied during reconstruction. A typical transversal slice of a high-resolution 7.0T is shown in Figure 1.

### 2.3. Visual rating of microbleeds

Both scans were visually scored a total of eight times (twice by four trained raters with experience in microbleed rating), using minimal intensity projection post-processing of both echo time images simultaneously. Processed images with a slab thickness of 2mm (no overlap), and images with a slab thickness of 4mm and a -2mm gap between the slices (2 mm overlap) were used for both scans. Microbleeds were defined as black, round lesions on the first or second echo image. If such lesions were visible on the first echo image, but were not larger on the second echo image, they were not scored as microbleeds, because of the missing blooming effect. Lesions were distinguished into possible or definite microbleeds, according to the Microbleed Anatomical Rating Scale (MARS) [9]. The scoring time for each scan per rater was recorded and averaged. The average scoring time was 31 minutes for participant 1 and 29 minutes for participant 2.

A lesion on a particular location was labeled as a definite microbleed for the ground truth rating if it had been labeled as such on at least 5 of the 8 ratings. Lesions that had been marked as definite microbleeds on 4 or less of the 8 ratings were examined in a consensus meeting and included or excluded as ground truth rating based on

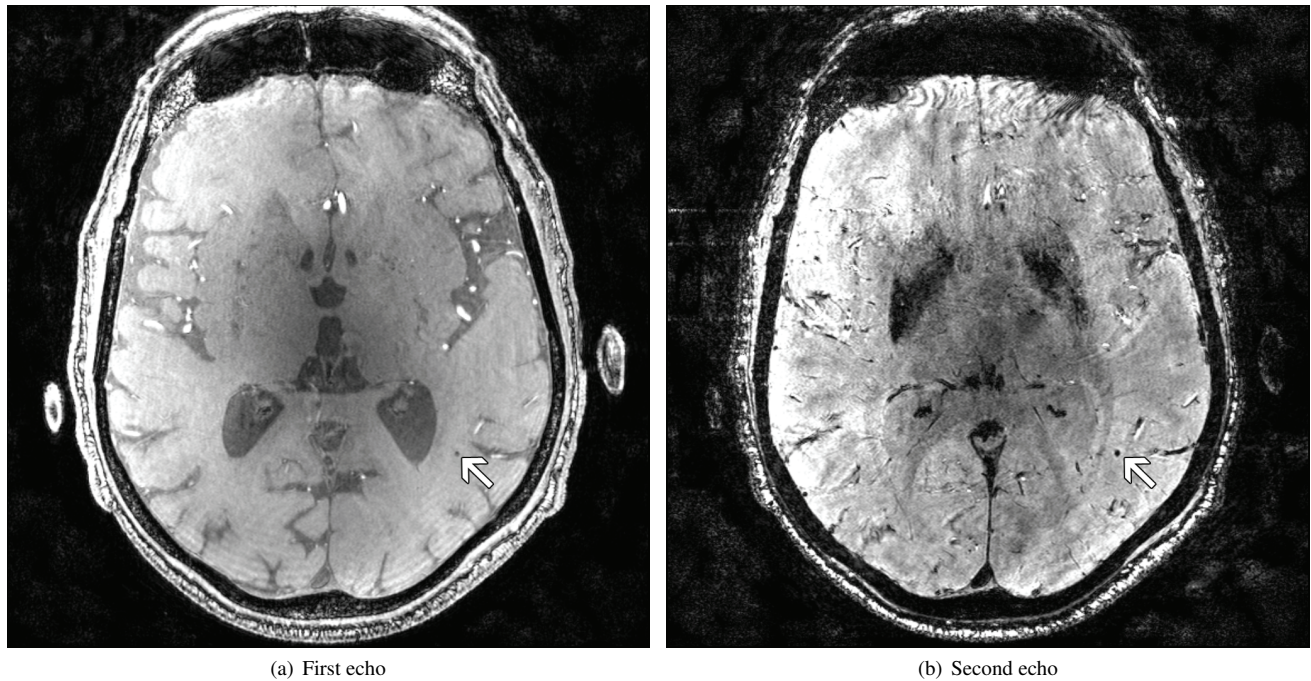


**Fig. 1.** A typical slice of a 7.0T T2\*-weighted MR scan, showing the first and second echo. The arrows annotate a microbleed.

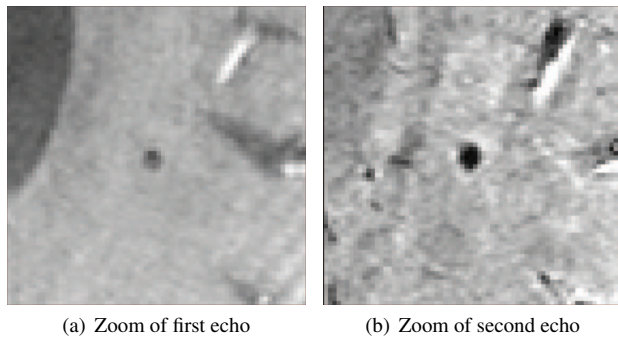


**Fig. 2.** Zoom on the microbleed of the first and second echo shown in Figure 1.

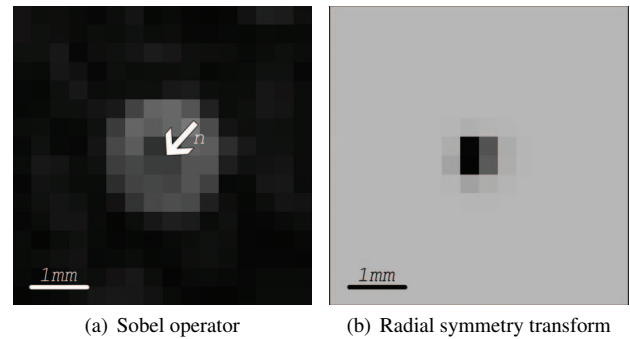


**Fig. 3.** Output of the Sobel operator and the radial symmetry transform on the first echo of the microbleed shown in Figures 1 and 2. The  $n$  in 3(a) shows a possible radius from the set  $N$ . When using smaller or larger  $n$ , the radial symmetry contribution does not sum up in a single voxel.

majority voting. Participant 1 had 2 microbleeds in the ground truth rating, which were observed 6 and 7 times respectively by the human raters. Participant 2 also had 2 microbleeds in the ground truth rating, which were observed 7 and 8 times respectively. A microbleed present in the ground truth rating is shown in more detail in Figure 2.

The location of each microbleed was stored in a list, together with the number of times it was detected. This list was used in order to quantitatively evaluate our automatic method.

#### 2.4. Radial symmetry transform

For the automatic detection of possible microbleeds, we implemented a 3D version of the radial symmetry transform as described

by Loy and Zelinsky. [10] The radial symmetry transform is a technique that utilizes local radial symmetry to highlight points of interest in an image.

The choice for a radial symmetry transform is derived from the properties of a cerebral microbleed on the MR scan. The actual hemosiderin deposit is very small [5], so it is safe to assume that the hemosiderin deposit is contained within a single voxel of the MR scan. The blooming effect of the microbleed, influenced by the echo time, is of equal strength in all directions, which creates a spherical hypointense spot in the scan. This perfectly fits into the concept of the radial symmetry transform.

The proposed method uses image gradients and orientations to infer the center of mass of each spherical object in the scan. The MR scans are preprocessed to normalize the gray-values into the same

**Table 1.** Results of the radial symmetry transform.  $\alpha$  is the radial strictness parameter and  $\beta$  the gradient threshold.  $T$  is the automatically determined threshold that keeps the true microbleeds in the results and #FP shows the number of false positives for participants 1 and 2, which needed to be removed by the human rater.

$\alpha$	$\beta = 2.5\%$			$\beta = 5.0\%$			$\beta = 7.5\%$			$\beta = 10.0\%$		
	$T$	#FP 1	#FP 2	$T$	#FP 1	#FP 2	$T$	#FP 1	#FP 2	$T$	#FP 1	#FP 2
1	-115	26	29	-115	26	29	-114	27	28	-114	23	28
2	-50	9	6	-50	8	6	-50	7	6	-50	7	7
3	-23	7	6	-23	7	6	<b>-23</b>	<b>6</b>	<b>4</b>	-22	6	4
4	-8	22	12	-8	20	11	-8	14	9	-8	9	7

range and the gradient information is computed using a 3D Sobel operator of size  $3 \times 3 \times 3$  voxels. To remove all responses of the transform in non-brain tissues, we used the Brain Extraction Tool (BET) [11] to create a brain-mask. The results of the BET were inspected visually to verify the correctness on the scans, but no manual corrections were needed. The result of the radial symmetry transform is mainly determined by three parameters: a set  $N$  of radii at which to compute the radial symmetry, the radial strictness parameter  $\alpha$ , and the gradient threshold  $\beta$  (see [10] for details).

The set of radii contains all radii of the microbleeds that can be present in the scan. Careful inspection of the individual microbleeds detected by the raters showed that the diameters range from approximately 0.7 to 2.8 mm. This corresponds with radii ranging from 1 to 4 voxels. Therefore, we choose our set  $N$  to include the radii  $\{1 \dots 2\}$  with a step size of 0.25 and the radii  $\{2 \dots 4\}$  with a step size of 0.5. These step sizes were chosen to account for possible partial volume effects, which can have a large influence on the results in small microbleeds.

The radial strictness parameter  $\alpha$  defines how strictly radial (or, in our case, spherical) the transform must be to return a high value. A value of 2 for  $\alpha$  is suggested [10], so in our experiments we varied  $\alpha$  to range from 1 to 4, with a step size of 1.

The gradient threshold  $\beta$  eliminates elements with small gradient magnitudes, because these result in less reliable orientations. We chose  $\beta$  to be 2.5%, 5%, 7.5%, or 10% of the highest gradient magnitude present in the image. These low values already eliminated a lot of noise and small variations in the scan, which did not correspond to microbleeds.

For each combination of  $\alpha$  and  $\beta$ , the sum of radial symmetry contributions for each radius  $n \in N$  at both echoes were computed separately. The gradient is calculated pointing from hypointense to hyperintense, so the output image  $S$  has positive values corresponding to bright spots and negative values corresponding to dark spots. An example of this is shown in Figure 3. In our datasets, microbleeds appear as dark, hypointense regions, so we ignored all positive values in  $S$ . The microbleeds were present at the same location in both echoes, so all locations that had a local minimum in  $S$  of the first and second echo were considered possible microbleed locations.

## 2.5. Experiments

In the experiments that were performed, the number of false positives present in the results was assessed together with the time a human rater required to visually indicate the false positives.

The radial symmetry was computed for each combination of  $\alpha$  and  $\beta$  on both echoes for both participants. For the output images  $S$ , a single optimal threshold  $T$  was determined automatically to extract all minima for both participants that might correspond to microbleeds. As the location of the true microbleeds is known,

it was possible to ensure that the applied threshold preserves the true microbleeds in  $S$  for both participants. Non-minimum suppression within a 3-voxel neighborhood was applied to remove multiple minima close to each other, and the number of false positives was counted on the resulting image.

For the optimal setting of  $\alpha$  and  $\beta$  (with the least false positives), one rater was presented  $S$  after thresholding with  $T$  and non-minimum suppression. For each detected location, the rater visually annotated if it was a definite microbleed. The rater was blinded for the original rating of the scans and the time it took to filter out the false positives was recorded.

## 3. RESULTS

The values in Table 1 show the number of false positives that had to be removed by the human rater after setting  $T$ , grouped per  $\beta$  value. Setting  $\alpha$  too low ( $\alpha = 1$ ) or too high ( $\alpha = 4$ ) resulted in many false positives; the optimal value for  $\alpha$  was 3. Varying  $\beta$  did not have a large influence on the results, the optimal value was 7.5%. A value of 10% was not chosen, as this increases the chance on false negatives. The optimal threshold  $T$  with the chosen  $\alpha$  and  $\beta$  was -23.

For the optimal setting ( $\alpha = 3$ ,  $\beta = 7.5\%$  and  $T = -23$ ), the results were presented to a human rater who required 1.5 and 1 minutes to remove all false positives in the results of participant 1 and 2, respectively.

## 4. DISCUSSION

Detecting all potential cerebral microbleeds using the radial symmetry transform on 7.0T MR scans, with a relatively low number of false positives, seems feasible. Given the large variety of locations in the brain at which a microbleed can occur, together with the effort it takes to visually detect microbleeds reliably, the automatic method showed a large reduction in rating time. Not all microbleeds were detected by all raters during the ground truth rating (mean number of detections is 7 out of 8), whereas the automatic method did detect all microbleeds. Therefore, the chance of a human rater accidentally missing a microbleed is reduced and the reliability of microbleed detection will increase with our semi-automated method.

The fact that a cerebral microbleed is visible on exactly the same location in the first and second echo of the dual-echo T2\*-weighted MR scan was used. The advantage of having a second echo available rules out a large number of false positives, which correspond to noise and other structures that have some radial symmetry but are no microbleeds. However, previous work by Conijn *et al.* [8] showed that 15.4% of the microbleeds are not visible on the first echo and 1.9% are not visible on the second echo. This could be a problem

when applying this method to more participants. On the other hand, the microbleeds that were missing on one of the echoes were very small: their mean diameter is  $0.78 \pm 0.18$  mm on the second echo. This makes it hard for a human rater to detect those microbleeds. In most other studies, such small microbleeds were even ignored [6].

The size of the microbleeds, ranging from 0.7 to 2.8 mm in diameter, is larger than the voxel size of  $0.35 \times 0.35 \times 0.3$  mm<sup>3</sup>, which gives rise to an appreciable partial volume effect. Some small microbleeds can consist almost completely of partial volume voxels, which is illustrated in Figure 2. This problem is taken care of by the step size used in the set of radii  $N$ . Using a larger step size on small microbleeds increased the chance that a true microbleed is missing in the results, inasmuch as the radial symmetry contribution might not add up in a single voxel. Larger microbleeds are not hampered by this issue, as they already have a larger and more distributed radial symmetry contribution by definition. The set of radii  $N$  can easily be extended to allow detection of larger microbleeds.

Varying  $\beta$  did not have a significant effect on the results. If  $\beta$  is set to higher values, the output of the Sobel operator at the microbleed locations might not exceed the  $\beta$  value, resulting in false negatives. If  $\beta$  is set too low, noise in the image will not be filtered out, resulting in many false positives. However, our results showed that  $\beta$  is quite robust, as varying it within reasonable limits did not influence the results. Inspection of the false positives showed that they occur mostly within blood vessels. Blood vessels are round and elongated structures that are curved by nature. At points of high curvature, there can be sufficient radial symmetry contribution in the accumulator space of the transform to be falsely detected as a microbleed.

Varying  $\alpha$  did have a large influence on the results, as was also suggested by the original method [10]. A value of 1 is too low, as it allows for bilateral symmetry and not strictly radial symmetry. Values of 4 and above, allowing only strictly radial symmetry, are too high. Because of the earlier mentioned partial volume effect, a microbleed is not perfectly spherical in an MR scan, so requiring strictly radial symmetry is not appropriate. The values of  $\alpha$  and  $\beta$  do not need to be changed for other patients, as their values are relatively stable.

Choosing a value for the threshold  $T$  was done automatically, based on the ground truth rating that was available for both scans.  $T$  was automatically chosen in such a way that all true positives in the scans were preserved. However, this is only based on the two used scans, which does not guarantee that this is a robust value for  $T$  that will work on other scans as well. This pilot study will be extended to evaluate the feasibility of applying the radial symmetry transform to detect potential microbleeds, in order to turn this proof of principle into a general microbleed detection method.

## 5. CONCLUSION

In this proof of principle we showed that it is feasible to use the radial symmetry transform on high-resolution brain MR images to semi-automatically detect cerebral microbleeds. The profit in rating time for our method is considerable, as it was reduced from 30 to 1.5 minutes compared to visual rating.

## 6. ACKNOWLEDGEMENTS

This work was financially supported by the project Care4Me (Co-operative Advanced REsearch for Medical Efficiency) in the framework of the EU research programme ITEA (Information Technology for European Advancement).

## 7. REFERENCES

- [1] Katherine A. Knudsen, Jonathan Rosand, Diane Karluk, and Steven M. Greenberg, "Clinical diagnosis of cerebral amyloid angiopathy: Validation of the Boston Criteria," *Neurology*, vol. 56, no. 4, pp. 537–539, 2001.
- [2] Joanna M. Wardlaw, Stephanie C. Lewis, Sarah L. Keir, Martin S. Dennis, and Susan Shenkin, "Cerebral Microbleeds Are Associated With Lacunar Stroke Defined Clinically and Radiologically, Independently of White Matter Lesions," *Stroke*, vol. 37, no. 10, pp. 2633–2636, 2006.
- [3] M. W. Vernooij, A. van der Lugt, M. A. Ikram, P. A. Wielopolski, W. J. Niessen, A. Hofman, G. P. Krestin, and M.M.B. Breteler, "Prevalence and risk factors of cerebral microbleeds: The rotterdam scan study," *Neurology*, vol. 70, no. 14, pp. 1208–1214, 2008.
- [4] Steven M Greenberg, Meike W Vernooij, Charlotte Cordonnier, Anand Viswanathan, Rustam Al-Shahi Salman, Steven Warach, Lenore J Launer, Mark A Van Buchem, and Monique MB Breteler, "Cerebral microbleeds: a guide to detection and interpretation," *The Lancet Neurology*, vol. 8, no. 2, pp. 165 – 174, 2009.
- [5] Franz Fazekas, Reinhold Kleinert, Gudrun Roob, Gertrude Kleinert, Peter Kapeller, Reinhold Schmidt, and Hans-Peter Hartung, "Histopathologic analysis of foci of signal loss on gradient-echo t2\*-weighted mr images in patients with spontaneous intracerebral hemorrhage: Evidence of microangiopathy-related microbleeds," *American Journal of Neuroradiology*, vol. 20, pp. 637–642, April 1999.
- [6] Charlotte Cordonnier, Rustam Al-Shahi Salman, and Joanna Wardlaw, "Spontaneous brain microbleeds: systematic review, subgroup analyses and standards for study design and reporting," *Brain*, vol. 130, no. 8, pp. 1988–2003, 2007.
- [7] P.C.G. Simons, A. Algra, M.F. van de Laak, D.E. Grobbee, and Y. van der Graaf, "Second manifestations of arterial disease (smart) study: Rationale and design," *European Journal of Epidemiology*, vol. 15, pp. 773–781, 1999, 10.1023/A:1007621514757.
- [8] M. M. A. Conijn, M. I. Geerlings, P. R. Luijten, J. J. Zwanenburg, F. Visser, G. J. Biessels, and J. Hendrikse, "Visualization of cerebral microbleeds with dual-echo t2\*-weighted magnetic resonance imaging at 7.0 t," *J. Magn. Reson. Imaging*, vol. 32, no. 1, pp. 52–59, 2010.
- [9] S. M. Gregoire, U. J. Chaudhary, M. M. Brown, T. A. Yousry, C. Kallis, H. R. Jager, and D. J. Werring, "The Microbleed Anatomical Rating Scale (MARS): Reliability of a tool to map brain microbleeds," *Neurology*, vol. 73, no. 21, pp. 1759–1766, 2009.
- [10] G. Loy and A. Zelinsky, "Fast radial symmetry for detecting points of interest," *IEEE Transactions on Pattern Analysis and Machine Intelligence*, vol. 25, no. 8, pp. 959–973, 2003.
- [11] S.M. Smith, "Fast robust automated brain extraction," *Human Brain Mapping*, vol. 17(3), pp. 143–155, November 2002.